






Quantified limits of the nuclear landscape

Léo Neufcourt ^{1,2} Yuchen Cao (曹宇晨)^{3,4} Samuel A. Giuliani ^{2,3} Witold Nazarewicz ^{2,4}
Erik Olsen ⁵ and Oleg B. Tarasov ³

¹*Department of Statistics and Probability, Michigan State University, East Lansing, Michigan 48824, USA*

²*Facility for Rare Isotope Beams, Michigan State University, East Lansing, Michigan 48824, USA*

³*National Superconducting Cyclotron Laboratory, Michigan State University, East Lansing, Michigan 48824, USA*

⁴*Department of Physics and Astronomy, Michigan State University, East Lansing, Michigan 48824, USA*

⁵*Institut d'Astronomie et d'Astrophysique, Université Libre de Bruxelles, 1050 Brussels, Belgium*



(Received 13 January 2020; accepted 30 March 2020; published 14 April 2020)

Background: The chart of the nuclides is limited by particle drip lines beyond which nuclear stability to proton or neutron emission is lost. Predicting the range of particle-bound isotopes poses an appreciable challenge for nuclear theory as it involves extreme extrapolations of nuclear masses well beyond the regions where experimental information is available. Still, quantified extrapolations are crucial for a wide variety of applications, including the modeling of stellar nucleosynthesis.

Purpose: We use microscopic nuclear global mass models, current mass data, and Bayesian methodology to provide quantified predictions of proton and neutron separation energies as well as Bayesian probabilities of existence throughout the nuclear landscape all the way to the particle drip lines.

Methods: We apply nuclear density-functional theory with several energy density functionals. We also consider two global mass models often used in astrophysical nucleosynthesis simulations. To account for uncertainties, Bayesian Gaussian processes are trained on the separation-energy residuals for each individual model, and the resulting predictions are combined via Bayesian model averaging. This framework allows to account for systematic and statistical uncertainties and propagate them to extrapolative predictions.

Results: We establish and characterize the drip-line regions where the probability that the nucleus is particle bound decreases from 1 to 0. In these regions, we provide quantified predictions for one- and two-nucleon separation energies. According to our Bayesian model averaging analysis, 7759 nuclei with $Z \leq 119$ have a probability of existence ≥ 0.5 .

Conclusions: The extrapolation results obtained in this study will be put through stringent tests when new experimental information on existence and masses of exotic nuclei becomes available. In this respect, the quantified landscape of nuclear existence obtained in this study should be viewed as a dynamical prediction that will be fine-tuned when new experimental information and improved global mass models become available.

DOI: [10.1103/PhysRevC.101.044307](https://doi.org/10.1103/PhysRevC.101.044307)

I. INTRODUCTION

Of the several thousand atomic nuclei thought to exist, only around 3000 have been experimentally observed, and only 286 are considered to be primordial nuclides (i.e., isotopes found on Earth that have existed in their current form since before Earth was formed). All nuclear species can be mapped on the chart of nuclides, or nuclear landscape. The landscape's boundaries, the particle drip lines, mark the end of nuclear binding. On the proton-rich side, the drip line has been reached experimentally all the way up to ${}_{93}\text{Np}$ [1]. On the other hand, the neutron drip line has been delineated only for light nuclei up to ${}_{10}\text{Ne}$ [2] and for heavier elements it is based on theoretical predictions.

Quantifying the limits of nuclear binding is important for understanding the origin of elements in the universe. In particular, the astrophysical rapid neutron capture (r-) process responsible for the generation of many heavy elements is believed to operate very closely to the neutron drip line; hence, the structure of very exotic nuclei directly impacts

the way the elements are produced in stellar nucleosynthesis [3]. A quantitative understanding of the r-process requires knowledge of nuclear properties and reaction rates of ~ 3000 very neutron-rich isotopes, many of which cannot be reached experimentally. The missing nuclear data for astrophysical simulations must be provided by massive extrapolations based on nuclear models augmented by the most recent experimental data. Here Bayesian machine learning, with its unified statistical treatment of all uncertainties, is the tool of choice when aiming at informed predictions including both a reduction of extrapolation errors and quantified bounds.

The global modeling of all nuclei, including complex exotic nuclei far from stability, is a challenging quest that requires control of many aspects of the nuclear many-body problem. For such a task, the microscopic tool of choice is nuclear density-functional theory (DFT) rooted in the mean-field approach [4]. During recent years, several global DFT mass tables have been calculated using different energy density functionals (EDFs): Skyrme [5–7], Gogny [8,9],

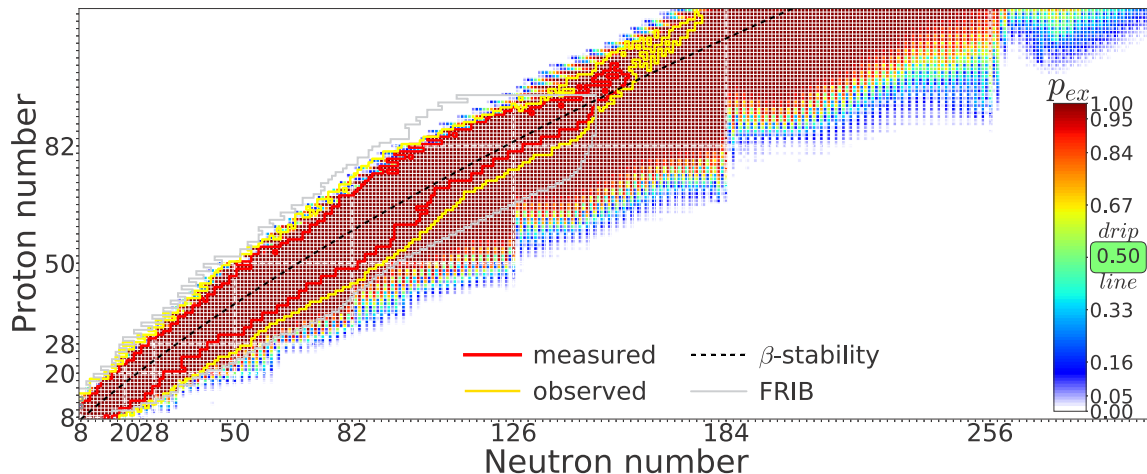


FIG. 1. The quantified landscape of nuclear existence obtained in our BMA calculations. For every nucleus with $Z, N \geq 8$ and $Z \leq 119$ the probability of existence p_{ex} (8), i.e., the probability that the nucleus is bound with respect to proton and neutron decay, is marked. The domains of nuclei which have been experimentally observed and whose separation energies have been measured (and used for training) are indicated. To provide a realistic estimate of the discovery potential with modern radioactive ion-beam facilities, the isotopes within FRIB’s experimental reach are marked. The magic numbers are shown by straight (white) dashed lines, and the average line of β -stability defined as in Ref. [51] is marked by a (black) dashed line. See text for details. This figure (without the FRIB range), in PDF format, can be downloaded from Ref. [32].

and covariant [7,10–12]. Other well-calibrated mass models include the microscopic-macroscopic finite-range droplet model (FRDM) [13] and Skyrme-HFB models based on the Hartree-Fock-Bogoliubov (HFB) method [14]. The number of predicted bound nuclides with atomic numbers between 2 and 120 shows significant model variations: For instance, it is around 7000 in the Skyrme-DFT analysis [5] while it is over 9000 in the covariant DFT approach of Ref. [12].

The systematic uncertainty on masses has often been estimated by an analysis of intermodel dependencies through comparing predictions of different DFT frameworks and different EDF parametrizations [5,7,15]. Statistical uncertainties are best evaluated by means of Bayesian inference methods involving full parameter estimation [16]. The uncertainties on calculated masses impact nuclear astrophysical calculations such as the r-process abundance predictions [3,17–19]. To improve the quality of theoretical mass predictions and minimize uncertainties, diverse machine learning techniques have been applied [20–26] that combine theoretical modeling with currently available experimental information.

In this study, we combine results of several global mass models and information contained in experimental masses to make a quantified assessment of proton and neutron separation energies and drip lines. To this end, we employ the technique of Bayesian model averaging (BMA) [27–29], which has recently been adopted to provide quantified predictions for both neutron-rich nuclei in the Ca region [30] and two-proton emitters [31].

The paper is organized as follows. Section II describes the nuclear mass models used and the statistical methodology adopted in our work. The results obtained in this study are discussed in Sec. III. Finally, Sec. IV contains a summary and conclusions. The tables of separation energies (with uncertainties) predicted in our BMA calculations are provided in the Supplemental Material [32] together with downloadable

plots of the quantified landscape of nuclear existence (Fig. 1) and the quantified separation energy landscape in the neutron drip-line region (Fig. 2) in PDF format.

II. METHODS

A. Nuclear mass models

In our study, we consider eight models based on nuclear DFT: the Skyrme energy density functionals SkM* [33], SkP [34], SLy4 [35], SV-min [36], UNEDF0 [37], UNEDF1 [38], and UNEDF2 [39] as well as the Gogny functional D1M [8] and the functional BCPM [40]. For each model, the mass table of even-even nuclei was computed self-consistently by solving the Hartree-Fock-Bogoliubov (HFB) equations as described in Refs. [5,26,30,31]; masses of odd- Z and odd- N systems were then extracted using computed pairing gaps [30,41].

The above set of DFT models was augmented by two mass-optimized mass models commonly used in nuclear astrophysics studies: the microscopic-macroscopic model FRDM-2012 [13] and the Skyrme-HFB model HFB-24 [14].

The above models were optimized using different strategies and varied datasets involving global nuclear observables and, sometimes, pseudodata such as nuclear matter parameters [4]. Consequently, the accuracy of these models with respect to measured masses [measured in terms of the root-mean-square (rms) deviation] varies between several MeV (SkM*) and ~ 600 keV (FRDM-2012 and HFB-24) [3]. Still, the rms mass deviations are reduced to similar values across models following statistical treatment, as demonstrated in Refs. [26,31].

B. Statistical methods

Our methodology follows closely our previous work [26,30,31] in which we combined the current theoretical

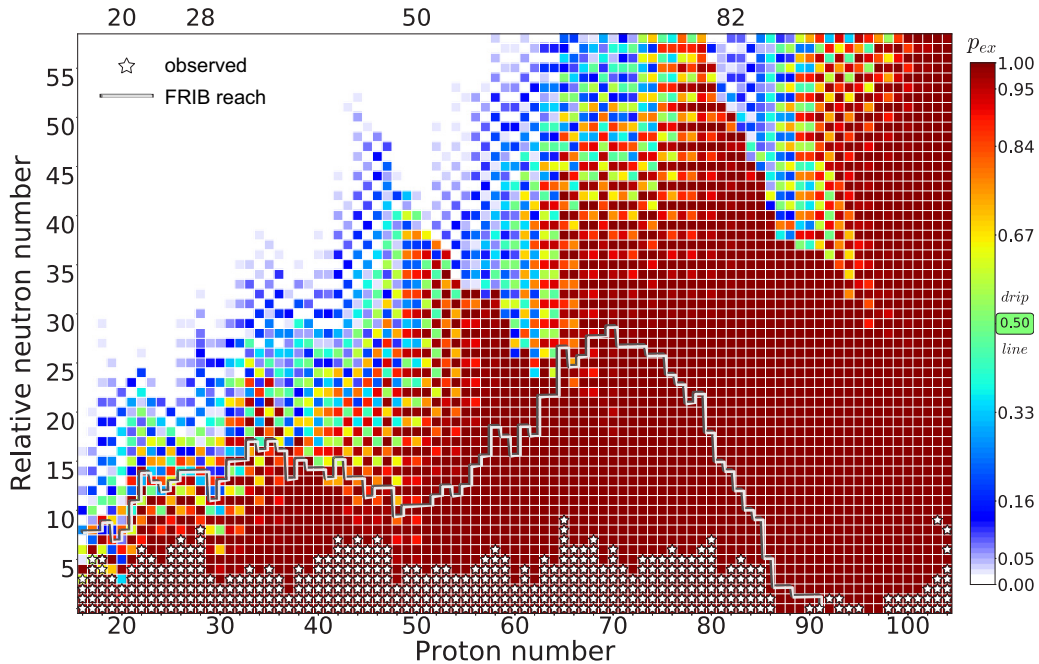


FIG. 2. The quantified separation energy landscape in the neutron drip-line region obtained with the BMA(n) model averaging. The color marks the “probability of existence” p_{ex} of neutron-rich nuclei, i.e., the probability that these nuclei are bound with respect to neutron decay. For each proton number, p_{ex} is shown along the isotopic chain versus the relative neutron number $N - N_0(Z)$, where $N_0(Z)$, listed in Table II, is the neutron number of the heaviest isotope for which an experimental one- or two-neutron separation energy value is available. The domain of nuclei that have been experimentally observed is marked by stars. To provide a realistic estimate of the discovery potential with modern radioactive ion-beam facilities, the isotopes within FRIB’s experimental reach are delimited by the shadowed solid line. See text for details. This figure (without the FRIB range), in PDF format, can be downloaded from Ref. [32].

and experimental information using Bayesian simulations to arrive at informed predictions.

1. Gaussian processes

The Bayesian statistical model for separation-energy residuals, i.e., differences $y_i = y^{\text{exp}}(x_i) - y^{\text{th}}(x_i)$ between experimental data and theoretical predictions, can be written as:

$$y_i = f(x_i, \theta) + \sigma \epsilon_i, \quad (1)$$

where the function $f(x, \theta)$ represents the systematic deviation and $\sigma \epsilon$ is the propagated statistical uncertainty.

Quantified extrapolations y^* are obtained from the posterior predictive distribution $p(y^*|y)$ using a stationary Markov chain. Similarly to our previous studies, we model independently S_{1n} , S_{2n} , S_{1p} , and S_{2p} on the four subsets of nuclei defined by the particle-number parities (even-even, even-odd, etc.). By doing this we are ignoring some (slight) correlations between systematic uncertainties.

For the function f we take a Gaussian process (GP) on the two-dimensional nuclear domain indexed by $x = (Z, N)$, characterized by its mean μ (taken here as a scalar parameter) and covariance k :

$$f(x, \theta) \sim \mathcal{GP}(\mu, k_{\eta, \rho}(x, x')). \quad (2)$$

The “spatial” dependence between nearby nuclei is represented by an exponential quadratic covariance kernel:

$$k_{\eta, \rho}(x, x') := \eta^2 e^{-\frac{(Z-Z')^2}{2\rho_Z^2} - \frac{(N-N')^2}{2\rho_N^2}}, \quad (3)$$

where the parameters η , ρ_Z , and ρ_N represent, respectively, the scale and characteristic correlation ranges in the proton and neutron directions. Consequently, our statistical model has four parameters $\theta := (\mu, \eta, \rho_Z, \rho_N)$. We have found in a previous study [26] that Gaussian processes overall outperform Bayesian neural networks, achieving similar rms deviations with a more faithful uncertainty quantification and considerably fewer parameters. We have also demonstrated [30,31] that the parameters θ are well constrained and fairly uncorrelated. It is worth noting that a nonzero value of the GP mean prediction μ allows to reproduce more consistently the extrapolative data. This GP extension to nonzero μ [31] significantly improves results.

2. Datasets

Our dataset combines all experimental masses from Atomic Mass Evaluations (AME) AME2003 [42] and AME2016 [43] augmented by the recently measured masses from Refs. [44–50]. For nuclei where experiments have been repeated, we take the most recent value. For testing purposes we split this dataset into a training set (AME2003) and a testing set (AME16-03: all masses in AME2016+ that are not in AME2003),

For prediction purposes, we use the full mass dataset for training—the performance of the statistical model was assessed in previous work [26,30,31]—and carry out calculations based on a large set of nuclei for which raw theoretical separation energies are not too negative; this includes

TABLE I. Model posterior weights obtained in the variants BMA(n) (4) and BMA(p) (5) of our BMA calculations. For compactness, the following abbreviations are used: UNEn = UNEDFn ($n = 0,1,2$) and FRDM = FRDM-2012.

BMA variant	SkM*	SkP	SLy4	SV-min	UNEO	UNE1	UNE2	BCPM	D1M	FRDM	HFB-24
BMA(n)	0.10	0.10	0.06	0.11	0.12	0.10	0.09	0.06	0.04	0.12	0.09
BMA(p)	0.00	0.03	0.08	0.05	0.04	0.14	0.12	0.04	0.16	0.17	0.17

all proton-bound nuclei. Nuclei with negative experimental separation energies, e.g., narrow ground-state proton resonances, have not been used for training.

3. Computations

Samples from posterior distributions were obtained from 50 000 iterations of Monte Carlo Markov chains, after the stationary state was reached (with 50 000 samples previously burnt-in), which were used in turn to generate 10 000 mass tables.

4. Bayesian model averaging

Based on general considerations [52], it is expected that BMA should on average outperform individual models. Similarly as in Refs. [30,31], also dealing with model-based extrapolations, in this study we employ the BMA framework to select the models with the best predictive power and avoid overfitting. This brings us to the BMA variants developed in our previous studies where the weight of each model \mathcal{M}_k is based on its capacity to account for known experimental data at the exterior of the training dataset.

We use two families of weights based on the data from the neutron-rich and proton-rich nuclear domains. On the neutron-rich side, we follow Ref. [30] and use the weights

$$w_k(n) : \propto p[S_{1n/2n}(x) > 0 | \mathcal{M}_k \text{ for } x \in \mathcal{D}_n], \quad (4)$$

where \mathcal{D}_n is the set of 254 experimentally observed neutron-rich nuclei with $20 \leq Z \leq 50$ for which no experimental neutron separation energy is available (such as ^{60}Ca [53]). On the proton-rich side, the experimental reach goes beyond the proton drip line, as separation energies have been established experimentally for many one- and two-proton emitters. To this end, in this region we follow Ref. [31] and use the weights given by

$$w_k(p) : \propto p[Q_{2p}(x) > 0, S_{1p}(x) > 0 | \mathcal{M}_k \text{ for } x \in \mathcal{X}_{2p}], \quad (5)$$

where \mathcal{X}_{2p} is the set of five long-lived two-proton emitters ^{19}Mg , ^{45}Fe , ^{48}Ni , ^{54}Zn , and ^{67}Kr (see Ref. [31] for more discussion). In the following, we refer to these variants as BMA(n) (4) and BMA(p) (5). To assess the whole landscape, we apply a local model averaging variant called BMA($n+p$), with local weights

$$w_k(Z, N) = w_k(n)H[N \geq N_\beta(Z)] + w_k(p)H[N < N_\beta(Z)], \quad (6)$$

where $H(x)$ is the Heaviside step function and $N_\beta(Z)$ is the neutron number corresponding to the average line of β stability defined as in Ref. [51].

III. RESULTS

The analysis of individual nuclear models' residuals in the context of theory developments has been discussed in, e.g., Ref. [26]. In this manuscript, we rather focus on quantified predictions of separation energies and drip lines, aiming to highlight the regions of the nuclear chart where the next-generation rare-isotope facilities may have the largest impact on theoretical modeling. The second goal is to provide predictions for drip lines with reliable uncertainties.

A. Model mixing

The model weights obtained in both BMA variants are listed in Table I. We can see that BMA(n) is well balanced between the models, while the BMA(p) is more selective. As discussed in Ref. [31], BMA(p) heavily penalizes large deviations at single locations.

By design, BMA($n+p$) retains the best of other two variants; it constitutes an innovative attempt for a principled local model averaging, which we called for in previous works [31,52]. Indeed, a model is arguably designed to reproduce a particular phenomenon of interest, and while the idea of universality is appealing, a dogmatic extension of a model to a wider domain can dangerously amount to overfitting. Local model averaging is particularly suited for situations where desired accuracy is high, and high-resolution effects must be taken into account to explain observations, in contrast to more qualitative descriptions.

In practice, all three BMA variants achieve a similar rms deviation ($S_{1n} \approx 302$ keV, $S_{2n} \approx 453$ keV, $S_{1p} \approx 410$ keV, $S_{2p} \approx 438$ keV), using AME16-03 as an independent (extrapolative) testing dataset (see Ref. [31] for methodology details).

While the theoretical statistical foundations of a general local averaging framework are yet to be set, in our simplified setup it corresponds to the hypothesis that neutron and proton separation energies are given by independent statistical models, which also matches our GP modeling assumption.

The BMA weights can be used to assess the relative predictive power of the individual models corrected with the GP: UNEDF0, FRDM-2012, and SV-min reach highest evidence on the neutron-rich side, and FRDM-2012, HFB-24, and D1M perform the best on the proton-rich side. Nevertheless, the relatively broad distribution of the weights suggests that no single model dominates.

B. Landscape of nuclear existence

Following Refs. [30,31] we compute the probability p_{ex} that a given isotope is particle-bound, i.e., that $S_{2p} > 0$ for even- Z nuclei, $S_{2n} > 0$ for even- N nuclei, $S_{1p} > 0$ for odd- Z nuclei, and $S_{1n} > 0$ for odd- N nuclei. Formally, this quantity

TABLE II. Table of the reference neutron numbers for even- Z nuclei (used in Fig. 2).

		Even- Z																					
Z :	16	18	20	22	24	26	28	30	32	34	36	38	40	42	44	46	48	50	52	54	56	58	60
N_0 :	29	30	37	35	40	42	45	52	54	57	61	64	67	69	73	77	83	85	88	92	93	93	100
Z :	62	64	66	68	70	72	74	76	78	80	82	84	86	88	90	92	94	96	98	100	102	104	
N_0 :	102	102	103	104	108	114	117	120	124	128	133	138	143	146	147	148	152	155	156	157	155	154	
		Odd- Z																					
Z :	17	19	21	23	25	27	29	31	33	35	37	39	41	43	45	47	49	51	53	55	57	59	
N_0 :	29	34	36	38	41	44	50	52	54	58	65	66	69	72	76	78	83	87	89	93	94	96	
Z :	61	63	65	67	69	71	73	75	77	79	81	83	85	87	89	91	93	95	97	99	101	103	
N_0 :	99	100	99	104	107	112	115	118	122	124	132	135	139	146	147	147	149	151	154	156	157	153	

can be defined as:

$$p_{ex} := p(S_{1p/2p/1n/2n}^* > 0 | S_{1p/2p/1n/2n}). \quad (7)$$

Since the proton and neutron drip lines are well separated, one can write:

$$p_{ex} = p(S_{1p/2p}^* > 0 | S_{1p/2p}) p(S_{1n/2n}^* > 0 | S_{1n/2n}), \quad (8)$$

where $p(S_{1p/2p}^* > 0 | S_{1p/2p})$ was obtained with $BMA(p)$ and $p(S_{1n/2n}^* > 0 | S_{1n/2n})$ —with $BMA(n)$.

The drip line corresponds to $p_{ex} = 0.5$. Figure 1 shows the posterior probability of existence p_{ex} for all nuclei in the nuclear landscape. The ranges of nuclear mass measurements and known nuclei are marked. To provide a representative example of discovery potential of next-generation radioactive ion beam facilities, the figure also shows the isotopes that will be accessible at the future Facility for Rare Isotope Beams (FRIB) [54,55].

The FRIB production rates have been estimated with the LISE++ code [56]. Production cross-sections for projectile fragmentation and fission reactions were obtained by using the EPAX2.15 cross-section systematics [57] and the LISE++3EER Abrasion-Fission model [58,59]. FRIB rates and details of their calculations are available online [60]. In our estimates, we assumed the experimental limit for the confirmation of existence of an isotope to be 1 event/2.5 days.

For neutron-rich nuclei, FRIB will approach the neutron drip line in the regions of neutron magic numbers. The magic nuclei are important for the r -process as they serve as major bottlenecks in the synthesis of heavier elements. In the region of proton-rich nuclei, due to the presence of the Coulomb barrier, relatively long-lived, proton-unstable nuclei can exist beyond the proton drip line [31,61]. As seen in Fig. 1, FRIB will reach the uncharted territory of many heavy proton-unstable nuclei.

To accompany Fig. 1, we tabulate in Ref. [32] the calculated posterior predictions for particle separation energies for all drip-line nuclei with $0.1 < p_{ex} < 0.9$.

C. Neutron-rich nuclei

The quantified separation energy landscape for neutron rich nuclei, predicted in $BMA(n)$, is displayed in Fig. 2. To facilitate the presentation, the information for each isotope is given relative to the neutron number N_0 of the heaviest

neutron-bound isotope for which an experimental one- or two-neutron separation energy value is available. The reference values of $N_0(Z)$ are listed in Table II. (For a similar diagram for proton-rich nuclei, see Ref. [31].) To illustrate how to read Fig. 2, we consider the Ni isotopic chain. The heaviest Ni isotope, for which mass has been measured is ^{73}Ni [62]; hence, $N_0(28) = 45$. The stars at $Z = 28$ indicate the isotopes $^{74-82}\text{Ni}$, which have been detected experimentally [63]. The nucleus ^{87}Ni is expected to have $p_{ex} < 50\%$, i.e., it is predicted to lie outside the one-neutron drip line. Because of pairing correlations, the two-neutron drip line for the Ni chain is shifted all the way to $N \approx 66$: The extremely neutron-rich isotope ^{92}Ni is predicted to be the last bound isotope.

Figure 2 also marks the reach of the FRIB facility, again as an example of what perhaps will be achievable experimentally. According to our analysis, FRIB will reach the one-neutron drip line up to $Z = 42$ (Mo) and will approach it again in the Sm-Gd region. For the Ni chain, the current phase of FRIB is expected to produce meaningful data on $^{86-87}\text{Ni}$. The use of fragmentation reactions will allow to study the existence of nuclides in the region of $Z = 16-24$, where the crucial check for theoretical models is provided by studying the neutron stability of ^{61}Ca [30].

As seen in Fig. 2, of particular importance for constraining theory are the existence data for $Z = 28-30$, $Z = 42-48$, and $Z = 64-66$. In all these cases, the one-neutron drip line is within experimental reach and theoretical uncertainties on the position of drip line are appreciable. The extension of mass measurements to more neutron-rich nuclei in the Ca-Ni and Cd-Sn regions will be of great value. Those can be carried out via the variety of methods, especially the time-of-flight technique [64] that can be applied to short-lived nuclides with 1–100 ms lifetimes.

D. Number of particle-bound nuclei

To estimate how many particle-bound nuclei exist in the nuclear landscape, we calculate the posterior distribution of the number of isotopes with positive one- and two-nucleon separation energies. We first produce such samples for each individual model, which are then resampled into BMA posterior distributions. These posterior distributions are shown in Fig. 3.

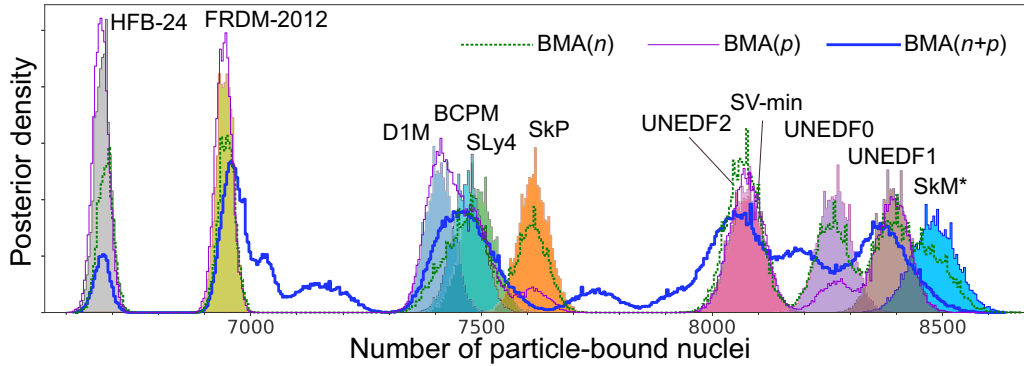


FIG. 3. Posterior distributions of the number of particle-bound nuclei. The histograms show the posterior densities for each model: the peaks correspond successively to HFB-24, FRDM-2012, D1M, BCPM, SLY4, SkP, SV-min and UNEDF2, UNEDF0, UNEDF1, and SkM*. The lines show the BMA posterior densities (multiplied by a constant factor 6.3 to facilitate presentation).

The number of nuclei with $Z, N \geq 8$ and $Z \leq 119$ predicted to be particle-bound by the individual models range from 6600 (HFB-24) to 8600 (SkM*). This difference comes from the neutron-rich heavy nuclei for which the extrapolation uncertainty is very significant. The BMA(n) distribution has its average at 7765 (± 590 standard deviation), with median at 8032 and centered 95% credibility interval [6669, 8516]. The BMA(p) distribution has its average at 7504 (± 602 standard deviation), with median at 7445 and centered 95% credibility interval [6661, 8425].

BMA($n+p$) amounts here to summing the number of neutron-rich nuclei obtained from the BMA(n) posterior distribution and the number of proton-rich nuclei obtained from the BMA(p) posterior distribution—hence the BMA($n+p$) distribution is a convolution of BMA(n) and BMA(p), which explains the smoothing effect seen in Fig. 3.

Accordingly, the values obtained from BMA($n+p$) lie in between with an average at 7708 (± 534 standard deviation) median at 7785 and centered 95% credibility interval [6688, 8440]. It is noticed that these bounds are tighter than those obtained with either BMA(n) or BMA(p).

Thus we can state without taking much risk that there should be between 6500 and 8500 stable nuclei based on the available mass data and models considered. While this result is consistent with the outcome of the earlier work [5] employing uniform model mixing, the present study provides for the first time the detailed posterior distribution of the number of nuclei bound for each model. This represents a significant refinement of previous work that has been allowed by our Bayesian statistical approach.

Figure 3 suggests that models can be clustered into three groups, where the more phenomenological ones yield the lowest number of particle-bound nuclei. Also, it is worth noting that the models with similar and high weights (such as UNEDF0 and FRDM-2012) predict rather different numbers of particle bound-nuclei. This is not too surprising: models tend to agree better in the domain of experimental data than at the location of the neutron drip line for the heaviest nuclei, where the available data allow only limited discrimination. It is expected that the future

mass data on neutron-rich nuclei will provide more model selectivity.

IV. CONCLUSIONS

By considering several global models and the most recent data on nuclear existence and masses, we applied novel Bayesian model averaging techniques to quantify the limits of the nuclear landscape. We hope the drip-line estimates as well as the specific predictions of one- and two-nucleon separation energies presented in this work will guide experimental research at next-generation rare isotope facilities. For instance, the posterior predictions of particle separation energies of drip-line nuclei tabulated in Ref. [32] can be useful when planning experiments aiming at establishing the existence of exotic isotopes. The related theoretical errors can guide the uncertainty analysis for the r -process abundance studies.

As we emphasized in previous studies [30,31], one should not expect that machine learning alone, however advanced, will somehow compensate for unknown systematic model deficiencies when extrapolating far away from the experimentally-established domain. Indeed, since the range of our extrapolations is 2 to 3 times larger than the fitted range of the correlation effects, we can expect the GP correction to the predictions, apart for the shift μ , to be relatively limited. Consequently, in the unknown regions, far extrapolations must rely on quality nuclear modeling. Therein, the honest evaluation of posterior predictive distributions is the key, i.e., the correction to the mean value is of less importance compared to credibility intervals. In this respect, the GP extension to nonzero μ as done in this work is perhaps more valuable than speculating about a more elaborate GP tail model, which—if not substantiated by physics—would not offer any obvious advantages.

In our BMA calculations, we applied three model-mixing techniques. Two of them, the local models BMA(n) and BMA(p), have been informed by the specific data on extreme nuclei pertaining to very different domains. Namely, for BMA(n) it is the existence of neutron-rich isotopes with unknown masses; for BMA(p) these are $2p$ separation energies of five true $2p$ emitters. The third global method BMA($n+p$)

retains locally each of these two variants on the part of the nuclear chart where it is, by design, expected to perform best.

According to our BMA($n + p$) analysis, the number of particle-bound nuclei with $Z, N \geq 8$ and $Z \leq 119$ is 7708 ± 534 . The results of the individual models shown in Fig. 3 show considerable spread, primarily due to the extrapolation uncertainty in the heavy neutron-rich region. This result underlines the fact that one should be very careful when trusting extrapolative predictions of any given model.

The extrapolations obtained in this study are timestamped. With the influx of new experimental data on existence and masses of exotic nuclei, and with new global mass models of high fidelity, the quantified landscape of nuclear existence will gradually evolve.

ACKNOWLEDGMENTS

Useful comments from Alexandra Gade are gratefully acknowledged. Computational resources for statistical simulations were provided to L.N. by the Institute for Cyber-Enabled Research at Michigan State University as well as Research Credits awarded by Google Cloud Platform. This material is based on work supported by the U.S. Department of Energy, Office of Science, Office of Nuclear Physics under Awards No. DE-SC0013365 (Michigan State University), No. DE-SC0018083 (NUCLEI SciDAC-4 collaboration), and No. DOE-NA0003885 (NNSA, the Stewardship Science Academic Alliances program).

-
- [1] Z. Y. Zhang *et al.*, New Isotope ^{220}Np : Probing the Robustness of the $N = 126$ Shell Closure in Neptunium, *Phys. Rev. Lett.* **122**, 192503 (2019).
- [2] D. S. Ahn *et al.*, Location of the Neutron Dripline at Fluorine and Neon, *Phys. Rev. Lett.* **123**, 212501 (2019).
- [3] C. J. Horowitz *et al.*, r -process nucleosynthesis: Connecting rare-isotope beam facilities with the cosmos, *J. Phys. G* **46**, 083001 (2019).
- [4] M. Bender, P.-H. Heenen, and P.-G. Reinhard, Self-consistent mean-field models for nuclear structure, *Rev. Mod. Phys.* **75**, 121 (2003).
- [5] J. Erler, N. Birge, M. Kortelainen, W. Nazarewicz, E. Olsen, A. Perhac, and M. Stoitsov, The limits of the nuclear landscape, *Nature* **486**, 509 (2012).
- [6] J. Erler, C. J. Horowitz, W. Nazarewicz, M. Rafalski, and P.-G. Reinhard, Energy density functional for nuclei and neutron stars, *Phys. Rev. C* **87**, 044320 (2013).
- [7] R. Wang and L.-W. Chen, Positioning the neutron drip line and the r -process paths in the nuclear landscape, *Phys. Rev. C* **92**, 031303(R) (2015).
- [8] S. Goriely, S. Hilaire, M. Girod, and S. Péru, First Gogny-Hartree-Fock-Bogoliubov Nuclear Mass Model, *Phys. Rev. Lett.* **102**, 242501 (2009).
- [9] J. P. Delaroche, M. Girod, J. Libert, H. Goutte, S. Hilaire, S. Péru, N. Pillet, and G. F. Bertsch, Structure of even-even nuclei using a mapped collective Hamiltonian and the D1S Gogny interaction, *Phys. Rev. C* **81**, 014303 (2010).
- [10] A. Afanasjev, S. Agbemava, D. Ray, and P. Ring, Nuclear landscape in covariant density functional theory, *Phys. Lett. B* **726**, 680 (2013).
- [11] S. E. Agbemava, A. V. Afanasjev, D. Ray, and P. Ring, Global performance of covariant energy density functionals: Ground state observables of even-even nuclei and the estimate of theoretical uncertainties, *Phys. Rev. C* **89**, 054320 (2014).
- [12] X. Xia, Y. Lim, P. Zhao, H. Liang, X. Qu, Y. Chen, H. Liu, L. Zhang, S. Zhang, Y. Kim, and J. Meng, The limits of the nuclear landscape explored by the relativistic continuum Hartree-Bogoliubov theory, *At. Data Nucl. Data Tables* **121-122**, 1 (2018).
- [13] P. Möller, A. Sierk, T. Ichikawa, and H. Sagawa, Nuclear ground-state masses and deformations: FRDM(2012), *At. Data Nucl. Data Tables* **109-110**, 1 (2016).
- [14] S. Goriely, N. Chamel, and J. M. Pearson, Further explorations of Skyrme-Hartree-Fock-Bogoliubov mass formulas. XIII. The 2012 atomic mass evaluation and the symmetry coefficient, *Phys. Rev. C* **88**, 024308 (2013).
- [15] A. V. Afanasjev, S. E. Agbemava, D. Ray, and P. Ring, Neutron drip line: Single-particle degrees of freedom and pairing properties as sources of theoretical uncertainties, *Phys. Rev. C* **91**, 014324 (2015).
- [16] J. D. McDonnell, N. Schunck, D. Higdon, J. Sarich, S. M. Wild, and W. Nazarewicz, Uncertainty Quantification for Nuclear Density Functional Theory and Information Content of New Measurements, *Phys. Rev. Lett.* **114**, 122501 (2015).
- [17] D. Martin, A. Arcones, W. Nazarewicz, and E. Olsen, Impact of Nuclear Mass Uncertainties on the r Process, *Phys. Rev. Lett.* **116**, 121101 (2016).
- [18] M. Mumpower, R. Surman, G. McLaughlin, and A. Aprahamian, The impact of individual nuclear properties on r -process nucleosynthesis, *Progr. Part. Nucl. Phys.* **86**, 86 (2016).
- [19] T. M. Sprouse, R. N. Perez, R. Surman, M. R. Mumpower, G. C. McLaughlin, and N. Schunck, Propagation of statistical uncertainties of Skyrme mass models to simulations of r -process nucleosynthesis, [arXiv:1901.10337](https://arxiv.org/abs/1901.10337) [Phys. Rev. C (to be published)].
- [20] S. Athanassopoulos, E. Mavrommatis, K. Gernoth, and J. Clark, Nuclear mass systematics using neural networks, *Nucl. Phys. A* **743**, 222 (2004).
- [21] R. Utama, J. Piekarewicz, and H. B. Prosper, Nuclear mass predictions for the crustal composition of neutron stars: A Bayesian neural network approach, *Phys. Rev. C* **93**, 014311 (2016).
- [22] R. Utama and J. Piekarewicz, Refining mass formulas for astrophysical applications: A Bayesian neural network approach, *Phys. Rev. C* **96**, 044308 (2017).
- [23] R. Utama and J. Piekarewicz, Validating neural-network refinements of nuclear mass models, *Phys. Rev. C* **97**, 014306 (2018).
- [24] H. F. Zhang, L. H. Wang, J. P. Yin, P. H. Chen, and H. F. Zhang, Performance of the Levenberg-Marquardt neural network approach in nuclear mass prediction, *J. Phys. G* **44**, 045110 (2017).
- [25] Z. Niu and H. Liang, Nuclear mass predictions based on Bayesian neural network approach with pairing and shell effects, *Phys. Lett. B* **778**, 48 (2018).
- [26] L. Neufcourt, Y. Cao, W. Nazarewicz, and F. Viens, Bayesian approach to model-based extrapolation of nuclear observables, *Phys. Rev. C* **98**, 034318 (2018).

- [27] J. A. Hoeting, D. Madigan, A. E. Raftery, and C. T. Volinsky, Bayesian model averaging: a tutorial (with comments by M. Clyde, David Draper and E. I. George, and a rejoinder by the authors), *Stat. Sci.* **14**, 382 (1999).
- [28] L. Wasserman, Bayesian model selection and model averaging, *J. Math. Psych.* **44**, 92 (2000).
- [29] J. M. Bernardo and A. F. M. Smith, Reference analysis, in *Bayesian Theory* (Wiley, New York, 1994).
- [30] L. Neufcourt, Y. Cao, W. Nazarewicz, E. Olsen, and F. Viens, Neutron Drip Line in the Ca Region from Bayesian Model Averaging, *Phys. Rev. Lett.* **122**, 062502 (2019).
- [31] L. Neufcourt, Y. Cao, S. Giuliani, W. Nazarewicz, E. Olsen, and O. B. Tarasov, Beyond the proton drip line: Bayesian analysis of proton-emitting nuclei, *Phys. Rev. C* **101**, 014319 (2020).
- [32] See Supplemental Material at <http://link.aps.org/supplemental/10.1103/PhysRevC.101.044307> for downloadable pdf versions of Figs. 1 and 2, and a table of posterior predictions of the separation energies of nuclei at the one-and two-particle drip lines.
- [33] J. Bartel, P. Quentin, M. Brack, C. Guet, and H.-B. Håkansson, Towards a better parametrisation of Skyrme-like effective forces: A critical study of the SkM force, *Nucl. Phys. A* **386**, 79 (1982).
- [34] J. Dobaczewski, H. Flocard, and J. Treiner, Hartree-Fock-Bogolyubov description of nuclei near the neutron-drip line, *Nucl. Phys. A* **422**, 103 (1984).
- [35] E. Chabanat, P. Bonche, P. Haensel, J. Meyer, and R. Schaeffer, New Skyrme effective forces for supernovae and neutron rich nuclei, *Phys. Scr.* **1995**, 231 (1995).
- [36] P. Klüpfel, P.-G. Reinhard, T. J. Bürvenich, and J. A. Maruhn, Variations on a theme by Skyrme: A systematic study of adjustments of model parameters, *Phys. Rev. C* **79**, 034310 (2009).
- [37] M. Kortelainen, T. Lesinski, J. Moré, W. Nazarewicz, J. Sarich, N. Schunck, M. V. Stoitsov, and S. Wild, Nuclear energy density optimization, *Phys. Rev. C* **82**, 024313 (2010).
- [38] M. Kortelainen, J. McDonnell, W. Nazarewicz, P.-G. Reinhard, J. Sarich, N. Schunck, M. V. Stoitsov, and S. M. Wild, Nuclear energy density optimization: Large deformations, *Phys. Rev. C* **85**, 024304 (2012).
- [39] M. Kortelainen, J. McDonnell, W. Nazarewicz, E. Olsen, P.-G. Reinhard, J. Sarich, N. Schunck, S. M. Wild, D. Davesne, J. Erler, and A. Pastore, Nuclear energy density optimization: Shell structure, *Phys. Rev. C* **89**, 054314 (2014).
- [40] M. Baldo, L. M. Robledo, P. Schuck, and X. Viñas, New Kohn-Sham density functional based on microscopic nuclear and neutron matter equations of state, *Phys. Rev. C* **87**, 064305 (2013).
- [41] Mass Explorer, <http://massexplorer.frib.msu.edu/>.
- [42] G. Audi, A. Wapstra, and C. Thibault, The AME2003 atomic mass evaluation: II. Tables, graphs and references, *Nucl. Phys. A* **729**, 337 (2003).
- [43] M. Wang, G. Audi, F. G. Kondev, W. J. Huang, S. Naimi, and X. Xu, The AME2016 atomic mass evaluation. II. Tables, graphs and references, *Chin. Phys. C* **41**, 030003 (2017).
- [44] A. de Roubin *et al.*, Nuclear deformation in the $A \approx 100$ region: Comparison between new masses and mean-field predictions, *Phys. Rev. C* **96**, 014310 (2017).
- [45] A. Welker *et al.*, Binding Energy of ^{79}Cu : Probing the Structure of the Doubly Magic ^{78}Ni from Only One Proton Away, *Phys. Rev. Lett.* **119**, 192502 (2017).
- [46] M. Vilen *et al.*, Precision Mass Measurements on Neutron-Rich Rare-Earth Isotopes at JYFLTRAP: Reduced Neutron Pairing and Implications for r -Process Calculations, *Phys. Rev. Lett.* **120**, 262701 (2018).
- [47] E. Leistenschneider *et al.*, Dawning of the $N = 32$ Shell Closure Seen Through Precision Mass Measurements of Neutron-Rich Titanium Isotopes, *Phys. Rev. Lett.* **120**, 062503 (2018).
- [48] S. Michimasa *et al.*, Magic Nature of Neutrons in ^{54}Ca : First Mass Measurements of $^{55-57}\text{Ca}$, *Phys. Rev. Lett.* **121**, 022506 (2018).
- [49] R. Orford *et al.*, Precision Mass Measurements of Neutron-Rich Neodymium and Samarium Isotopes and Their Role in Understanding Rare-Earth Peak Formation, *Phys. Rev. Lett.* **120**, 262702 (2018).
- [50] Y. Ito *et al.*, First Direct Mass Measurements of Nuclides Around $Z = 100$ with a Multireflection Time-of-Flight Mass Spectrograph, *Phys. Rev. Lett.* **120**, 152501 (2018).
- [51] T. Kodama, β -stability line and liquid-drop mass formulas, *Prog. Theor. Phys.* **45**, 1112 (1971).
- [52] V. Kejzlar, L. Neufcourt, T. Maiti, and F. Viens, Bayesian averaging of computer models with domain discrepancies: A nuclear physics perspective, [arXiv:1904.04793](https://arxiv.org/abs/1904.04793).
- [53] O. B. Tarasov *et al.*, Discovery of ^{60}Ca and Implications for the Stability of ^{70}Ca , *Phys. Rev. Lett.* **121**, 022501 (2018).
- [54] T. Glasmacher, B. Sherrill, W. Nazarewicz, A. Gade, P. Mantica, J. Wei, G. Bollen, and B. Bull, Facility for rare isotope beams update for nuclear physics news, *Nucl. Phys. News* **27**, 28 (2017).
- [55] B. M. Sherrill, Future opportunities at the facility for rare isotope beams, *EPJ Web Conf.* **178**, 01001 (2018).
- [56] O. B. Tarasov and D. Bazin, Lise++: Radioactive beam production with in-flight separators, *NIM B* **266**, 4657 (2008).
- [57] K. Sümmerer and B. Blank, Modified empirical parametrization of fragmentation cross sections, *Phys. Rev. C* **61**, 034607 (2000).
- [58] O. B. Tarasov, LISE++ development: Abrasion-Fission, *Eur. Phys. J. A* **25**, 751 (2005).
- [59] O. B. Tarasov, LISE++ development: Abrasion-Fission, Tech. Rep. **MSUCL1300** (2005), http://lise.nsl.msu.edu/7_5/lise++_7_5.pdf.
- [60] FRIB Estimated Rates, <https://groups.nsl.msu.edu/frib/rates/fribrates.html>.
- [61] M. Pfützner, M. Karny, L. V. Grigorenko, and K. Riisager, Radioactive decays at limits of nuclear stability, *Rev. Mod. Phys.* **84**, 567 (2012).
- [62] S. Rahaman *et al.*, Masses of neutron-rich Ni and Cu isotopes and the shell closure at $Z = 28, N = 40$, *Eur. Phys. J. A* **34**, 5 (2007).
- [63] T. Sumikama, S. Nishimura, H. Baba, F. Browne, P. Doornenbal, N. Fukuda, S. Franchoo, G. Gey, N. Inabe, T. Isobe, P. R. John, H. S. Jung, D. Kameda, T. Kubo, Z. Li, G. Lorusso, I. Matea, K. Matsui, P. Morfouace, D. Mengoni, D. R. Napoli, M. Niikura, H. Nishibata, A. Odahara, E. Sahin, H. Sakurai, P. A. Soderstrom, G. I. Stefan, D. Suzuki, H. Suzuki, H. Takeda, R. Taniuchi, J. Taprogge, Z. Vajta, H. Watanabe, V. Werner, J. Wu, Z. Y. Xu, A. Yagi, and K. Yoshinaga, Observation of new neutron-rich Mn, Fe, Co, Ni, and Cu isotopes in the vicinity of ^{78}Ni , *Phys. Rev. C* **95**, 051601(R) (2017).
- [64] M. A. Famiano, Nuclear mass measurements with radioactive ion beams, *Int. J. Mod. Phys. E* **28**, 1930005 (2019).